ACS OMEGA

http://pubs.acs.org/journal/acsodf

Article

Triboelectrification-Induced Electricity in Self-Healing Hydrogel for Mechanical Energy Harvesting and Ultra-sensitive Pressure Monitoring

Kun Zhao,* Haoran Lv, Jingke Meng, Zhenhua Song, Cheng Meng, Maocheng Liu,* and Ding Zhang*

Cite This: *ACS Omega* 2022, 7, 18816−18825

Read Online

ACCESS | Metrics & More | Article Recommendations | Supporting Information

ABSTRACT: Triboelectric nanogenerators (TENGs) have shown huge application potential in the fields of micro−nano energy harvesting and multifunctional sensing. However, the damage of triboelectric material is one of the challenges for their practical applications. Herein, we fabricated a flexible TENG employing self-healing hydrogel and fluorinated ethylene propylene film as triboelectric materials for mechanical energy harvesting and pressure monitoring. The prepared hydrogel not only has excellent flexibility, transparency, and self-healing property but also exhibits good mechanical property without plastic deformation and damage under a large stretchable strain of 200%. The output electric signals of TENGs are as high as 33.0 V and 3 μA under a contact frequency of 0.40 Hz and a pressure of 2.9 N, respectively, which can charge a capacitor of 0.22 μF to 24.3 V within 300 s. Note that the voltage retention rate of TENGs after self-healing is up to 88.0%. Moreover, hydrogel-based TENGs can act as a wearable pressure sensor for monitoring human motion, exhibiting a high sensitivity of 105.9 mV/N or 1.73 nA/N under a contact frequency of 0.40 Hz. This research provides a reference roadmap for designing TENGs and self-powered pressure sensors with flexibility, self-healing, and robustness.

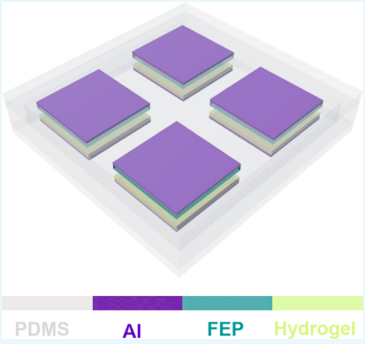

1. INTRODUCTION

As technology continues to advance, flexible wearable electronics gradually show huge application potential in electronic skin (E-skin),[1,2] soft robotics,[3,4] health monitoring,[5,6] and other aspects in human daily lives.[7] However, as traditional power supply methods, batteries and capacitors require frequent charging and maintenance due to limited capacitance, which affect the continuous operation and stability of wearable electronics, especially in harsh environments.[8,9] At the same time, discarded batteries/capacitors also cause serious pollution to the environment.[10−14] Therefore, developing high-performance sustainable energy technologies becomes one of the important research topics. In 2012, Wang's group first invented the triboelectric nanogenerator (TENG) that can convert various kinds of mechanical energies into electrical energy for self-powered electronics,[15] such as human motion energy,[16] vibration energy,[17,18] wind energy,[19,20] rain drop energy,[21] water wave energy,[22,23] and sound energy.[24,25] With continuous research and progress, the output performance of TENGs have been greatly improved,[26−34] which facilitates their practical process in daily life. It plays a very good supplementary role to traditional energy and is of great significance to the realization of carbon neutrality goals.

As a new intrinsically conductive material, polymeric hydrogels have adjustable conductivity, excellent self-healing performance, and good biocompatibility, thus showing great potential applications in soft robots, biomimetic prostheses, health monitoring, and wearable electronics.[35−38] The hydrogel-based TENGs have already attracted great attention and obtained satisfactory achievement by hydrogel structure design and optimization.[39−42] Pu et al. fabricated a flexible sandwich-structured TENG based on a polyacrylamide hydrogel as an electrode for harvesting biomechanical energy and acting as an E-skin.[41] However, this TENG does not possesses self-healing property and cannot work normally after damage. Sun et al. developed a polyacrylamide/gelatin/PEDOT:PSS composite hydrogel that has good flexibility, stretchability, and sensitivity to stress.[42] As the electrode of a sandwich-structured TENG, only the hydrogel has good self-healing property, and TENG cannot work normally when the charged layer is damaged. In addition, a linear silicone-modified polyurethane coating and a temperature-responsive polycaprolactone film as self-healing friction layers have been used to fabricate TENGs, which is of great significance to prolong the service life of TENGs.[43,44] Thus far, there are no reports on the use of self-healing hydrogels as triboelectric materials to fabricate TENGs.

Here, we report a novel TENG based on a flexible and transparent hydrogel with excellent self-healing property directly as a triboelectric material, which shows great potential for a

Received: March 23, 2022
Accepted: May 13, 2022
Published: May 26, 2022

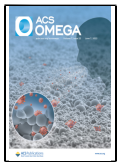

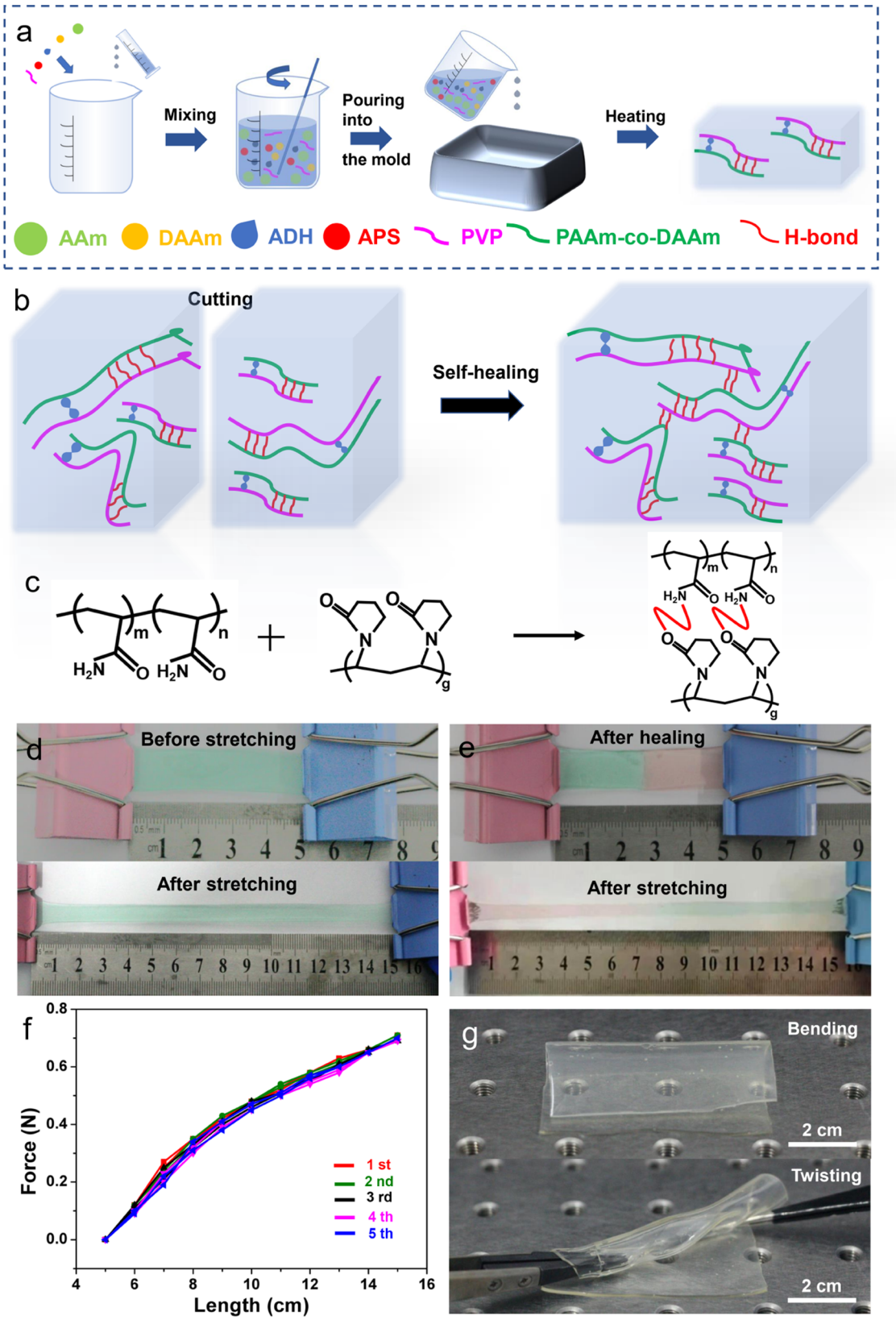

Figure 1. (a) Schematic diagram for the preparation process of the self-healing hydrogel. (b,c) Self-healing principle diagram of the hydrogel. (d) Demonstration of tensile property of the self-healing hydrogel. (e) Demonstration of tensile property of the self-healing hydrogel after self-healing. (f) Stretched length and corresponding tensile force curves of self-healing hydrogel from the first to fifth stretches. (g) Demonstration of flexibility of self-healing hydrogel: bending and twisting.

broad range of applications in mechanical energy harvesting and pressure monitoring. After being stretched to 200% strain, the hydrogel still shows good mechanical performance without plastic deformation. After a complete self-healing process, a cut

https://doi.org/10.1021/acsomega.2c01743
ACS Omega 2022, 7, 18816−18825

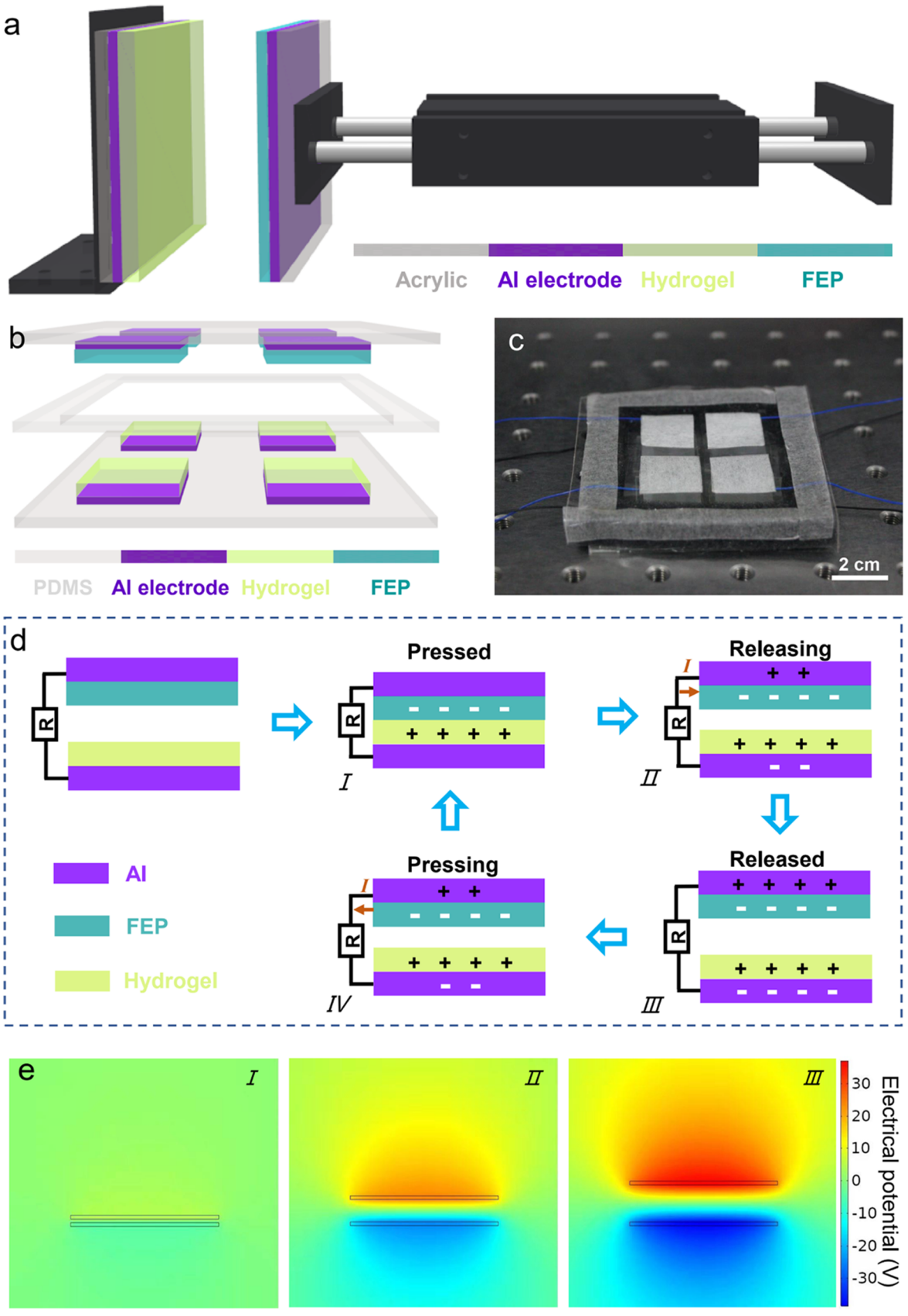

Figure 2. (a,b) Schematic diagram of the self-healing hydrogel-based TENG (a) and pressure array sensor (b). (c) Photograph of the pressure array sensor. (d) Working principle of TENG. (e) Simulation calculations of the electric potential distribution of TENG between contacting interfaces by COMSOL software.

https://doi.org/10.1021/acsomega.2c01743
ACS Omega 2022, 7, 18816−18825

hydrogel as the friction material can still give TENG high output performance with a large voltage retention rate of 88%. A hydrogel-based wearable array sensor exhibits a high sensitivity of 105.9 mV/N or 1.73 nA/N, showing great application potential in self-powered wearable sensing systems.

2. EXPERIMENTAL SECTION

2.1. Preparation of Self-Healing Hydrogels. The self-healing hydrogels were prepared using a simple one-pot method. Typically, acrylamide (AM) (7.029 g) and diacetone acrylamide (DAAM) (0.169 g) were added into a distilled water solution (20 mL) and stirred well. Then, polyvinylpyrrolidone (PVP-K30, $M_w = 5.0 \times 10^4$ g/mol) (0.34 g), adipic dihydrazide (ADH) (0.087 g), and ammonium persulfate (APS) (0.05 g) were added in the above mixed solution in sequence. After stirring for 1 h and standing for 3 h, the solution was poured into glass molds measuring 8 × 7 × 1 mm and protected with nitrogen and then heated at 40 °C for 6 h to obtain a self-healing hydrogel with a thickness of 1 mm.

2.2. Fabrication of the TENG and Sensor. First, the self-healing hydrogel, fluorinated ethylene propylene (FEP) film, and aluminum (Al) foil were cut into squares with dimensions of 5.0 × 5.0 cm each. Then, using a laser cutting machine, two acrylic plates were cut with dimensions of 6.0 × 6.0 cm as supports. Finally, the cut Al electrode and triboelectric materials were closely adhered to the acrylic plates to construct the TENG.

A 2 × 2 sensor array consists of 4 small TENGs with a size of 2.0 × 2.0 cm, in which the back of the TENG electrode is supported by PDMS with a size of 8.0 × 8.0 cm × 200 μm, the distance between each sensor unit is 1 cm, and the device is surrounded by elastic sponge as a flexible support.

2.3. Characterization and Measurement. Infrared spectra were recorded on a Fourier transform infrared (FTIR, Nexus 670) spectrometer from 400 to 4000 cm^{-1}. Measurement of lyophilized samples of self-healing hydrogels was done using the KBr particle method. The morphologies of the hydrogel were observed using a scanning electron microscope (Quanta 450) and a laser scanning confocal microscope (LSM800 Carl Zeiss, Germany). The force was provided by a linear motor (LinMot 1100) and measured by a force sensor (BSCC-H2). The output voltage and current signals of the TENG were obtained by using a mixed domain oscilloscope (Tektronix MDO3014) and a system electrometer (Keithley 2611B), respectively.

3. RESULTS AND DISCUSSION

Figure 1a shows the preparation process of the self-healing hydrogel. Using APS as an initiator, AM and DAAM as monomers were free-radically copolymerized to form long chains of PAM-*co*-DAAM. The ketone group in the long chain reacts with the hydrazide of ADH to form an acylhydrazone bond as the first cross-linking point and can improve the toughness and stretchability of the hydrogel.[45] Moreover, PVP can synergize with the $CONH_2$ functional groups of PAM-*co*-DAAM to generate hydrogen bonds to form a second cross-link.[46] The FTIR spectrum of the hydrogel shows that the stretching bands at 3435, 1630, and 1097 cm^{-1} correspond to the characteristic absorption bands of O−H, C═O, and C−N in ADH, respectively (Figure S1). The self-healing principle of the hydrogel is displayed in Figure 1b. When the hydrogel is cut, owing to the hydrogen bonds between PVP chains and the $CONH_2$ functional groups of PAM-*co*-DAAM, the hydrogel can be repaired spontaneously without external interference. After self-healing for 12 h, the two hydrogels can self-heal well under the dynamic cleavage and reconstruction of hydrogen bonds and the rearrangement of polymer segments. The process of forming hydrogen bonds is shown in Figure 1c.

Note that the obtained hydrogel has a typical porous network morphology of the gel matrix after freeze-drying, indicating the formation of the hydrogel (Figure S2a,b). Also, the LSCM images showed that the surface of the hydrogel before freeze-drying was smooth (Figure S2c,d). To examine the tensile properties of the hydrogels, the prepared hydrogels with a thickness of 1.0 mm were dyed red and green, respectively, and then cut into strips of 1.0 × 6.0 cm (Figure S3a). The two ends were clamped for 0.5 cm and then slowly stretched. As can be seen from Figures 1d and S4, the clamped hydrogels can be stretched from 5.0 to 15.0 cm with a stretchable strain of 200%. Note that when the two hydrogels were cut from the middle (Figure S3b), self-healing process could be completed within 12 h and the original tensile properties could be maintained (Figure 1e). To explore the mechanical properties of the hydrogel, the relationship between the stretched length of the hydrogel and corresponding tensile force was measured. As shown in Figure 1f, the hydrogel with a width of 1.0 cm was gradually elongated from 5.0 to 15 cm, and the tensile force was also gradually increased from 0 to 0.71 N. During the recovery process, the pulling force was gradually reduced from 0.71 to 0 N, showing excellent stability for 5 cycles. This indicates that the hydrogel has good elastic deformation properties without irreversible deformation during the stretching-recovery process from 5.0 to 15.0 cm. In addition, the photographs of the prepared self-healing hydrogels in the bending and twisting states are displayed in Figure 1g, showing good transparency and excellent flexibility.

To further explore the application value of the self-healing hydrogel in energy-harvesting and self-powered sensing system, we designed a TENG and a wearable pressure sensor based on the hydrogel, respectively. Figure 2a shows the schematic diagram of the TENG with a contact-separation mode fixed on a linear motor. The self-healing hydrogel and FEP film were used as triboelectric materials with a size of 5.0 × 5.0 cm, Al foils were used as electrodes, and acrylic sheets were used as support materials. Figure 2b,c shows the structure diagram and optical image of the wearable pressure sensor, which contains four TENGs individually with the size of 2.0 × 2.0 cm. Figure 2d is a schematic diagram of the working principle of the TENG. Its work process can be divided into four steps: (I) When pressing the TENG, the FEP film contacts with the hydrogel film, and the equal and opposite charges are generated on the surface of FEP (negative charge) and hydrogel (positive charge) films due to the triboelectrification. (II) When removing the external force, the FEP film separates from the hydrogel film. Owing to electrostatic induction, the electron flows from the upper Al electrode to the bottom Al electrode, and the opposite charges are generated on two Al electrodes, while negative charges are generated by the FEP film. In this process, a current was produced from the bottom to upper electrodes. (III) When the FEP film recovers to its original state, there is no electron flow between the two electrodes owing to the electrostatic balance. (IV) when pressing the TENG again, the electrostatic balance is broken, and the electron flows from the bottom to the upper Al electrode, corresponding to an opposite current direction compared with step II. The potential difference and potential

https://doi.org/10.1021/acsomega.2c01743
ACS Omega 2022, 7, 18816−18825

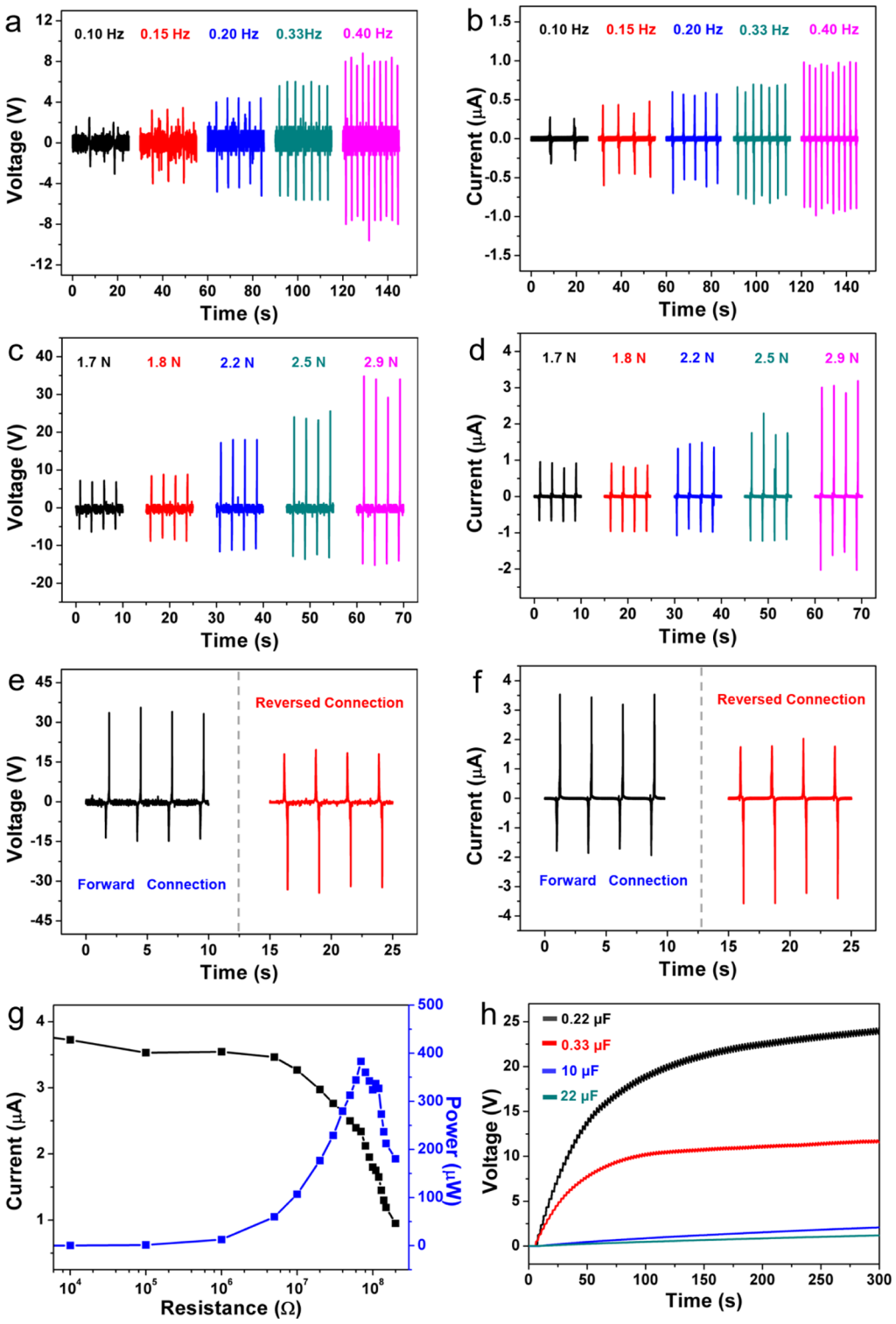

Figure 3. (a,b) Measured output voltage (a) and current (b) signals of TENG under different frequencies (0.10−0.40 Hz) at 1.7 N. (c,d) Measured output voltage (c) and current (d) signals of TENG under different pressures (1.7−2.9 N) at 0.40 Hz. (e,f) Measured output voltage (e) and current (f) signals of TENG under forward connection and reversed connection at 2.9 N and 0.40 Hz. (g) Measured output currents and calculated output powers of TENG under different loads at 2.9 N and 0.40 Hz. (h) Charging curves of capacitors with different capacitances driven by TENG at 2.9 N and 0.40 Hz.

distribution of the two electrodes of the TENG were theoretically simulated using COMSOL modeling, and the results are shown in Figure 2e.

To measure the output performance of the hydrogel-based TENG with a size of 5.0 × 5.0 cm (Figure 2a) under different conditions, we systematically studied the output voltages and currents of the TENG under different working frequencies and forces. First, we measured the effect of different frequencies on the output performance of the device at 1.7 N. As shown in Figure 3a,b, as the contact frequencies gradually increased from

https://doi.org/10.1021/acsomega.2c01743
ACS Omega 2022, 7, 18816−18825

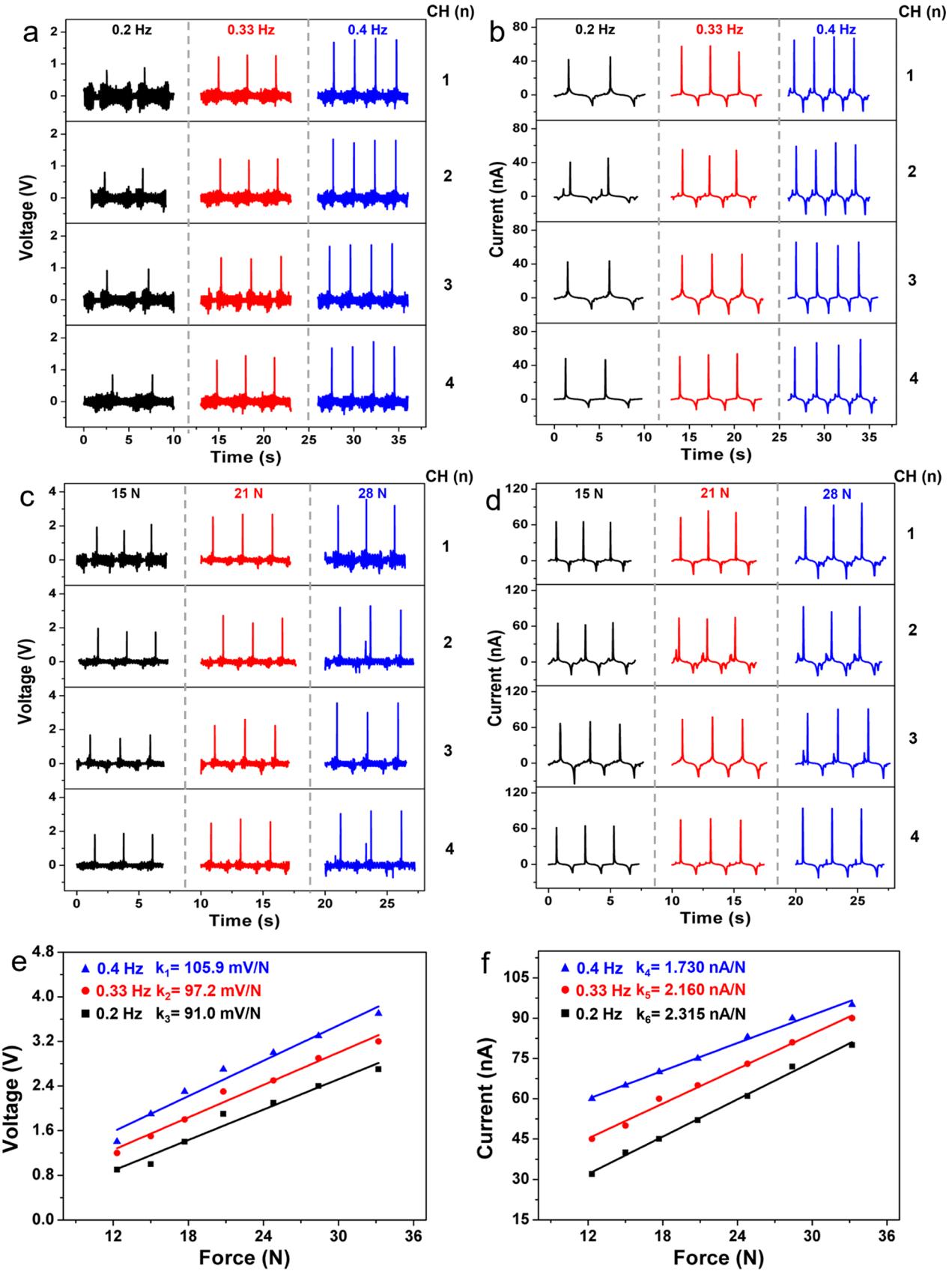

Figure 4. (a,b) Measured output voltage (a) and current (b) signals of the four channels of the sensor under different frequencies at 15 N. (c,d) Measured output voltage (c) and current (d) signals of the four channels of the sensor under different pressures at 0.40 Hz. (e) Linear fitting curves between the output voltages and pressures of the sensor under different frequencies. (f) Linear fitting curves between the output currents and pressures of the sensor under different frequencies.

https://doi.org/10.1021/acsomega.2c01743
ACS Omega 2022, 7, 18816−18825

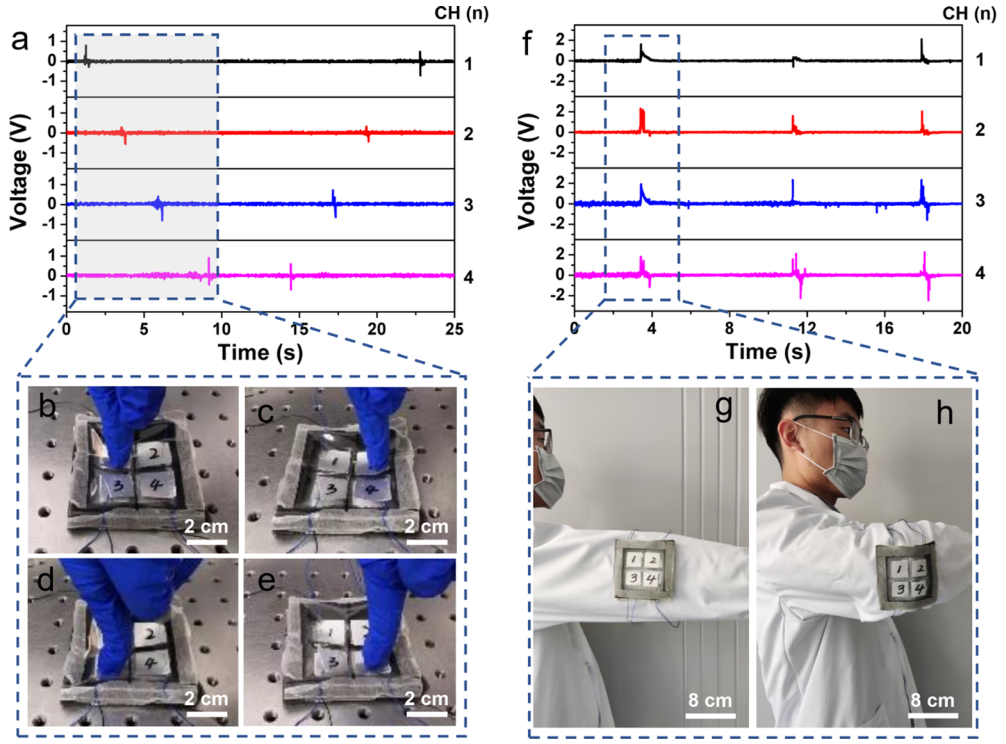

Figure 5. (a) Measured output voltage signals of the sensor when the right index finger presses the four channels in turn. (b−e) Photographs of the right index finger pressing sensor channel 1 (b), channel 2 (c), channel 3 (d), and channel 4 (e). (f) Measured output voltage signals of the four channels of the sensor when the elbow is flexed. (g,h) Photographs of the person wearing a sensor, straightening (g) and flexing (h) the elbow.

0.10 to 0.40 Hz, the open-circuit voltages/short-circuit currents increased from 2.0 V/0.3 μA to 8.0 V/0.9 μA, respectively. The improvement of the output performance is attributed to the increase of the electrostatic induction rate induced by the faster contact frequency, thus increasing the charges migration rate. Then, we further studied the output performance of the TENG under different pressure conditions and a constant contact frequency of 0.40 Hz. With the increase of the forces from 1.7 to 2.9 N, the corresponding output voltages/currents increase from 7.0 V/0.9 μA to 33.0 V/3.0 μA, respectively (Figure 3c,d). This is due to the increase of the contact area and degree between the hydrogel and the FEP film, which promotes the charge generation, thereby enhancing the output performance. The above research illustrates that the hydrogel-based TENG is sensitive to contact frequency and pressure, showing huge application potential in frequency and pressure monitoring. To determine the authenticity of the output signals of TENG, the circuit is connected through forward and reverse connections. The output performance of the TENG with the two connection modes above were measured under a pressure of 2.9 N and a contact frequency of 0.40 Hz (Figure 3e,f). The output voltages/currents are approximately 34.0 V/3.5 μA and −34.0 V/−3.5 μA, respectively. Despite the change in the circuit's forward and reverse connections, the absolute values of output electrical signals were unchanged, which confirms the authenticity of the output signals. It is worth noting that there is no obvious wear phenomenon on the hydrogel surface when the TENG runs continuously for 6 h (Figure S5), indicating that the device has good stability. In addition, in order to test the output performance change of the hydrogel-based TENG before cutting and after self-healing, the TENGs were constructed using the hydrogel before cutting and after self-healing as the triboelectric materials (Figure S6), respectively. Figure S7a,b shows the output voltage and current signals of the TENGs under a pressure of 2.9 N and a frequency of 0.40 Hz, the open-circuit voltage is reduced from 34.0 V before cutting to 30.0 V after self-healing, and the corresponding short-circuit current is reduced from 3.0 to 2.5 μA. It can be seen from the calculations that the output voltage and current retention rates of the TENG fabricated with the self-healed hydrogel current are as high as 88 and 83%, respectively, indicating excellent stability of the TENG. Note that both the output voltages and currents of the TENG increased with the increase of healing time, and when the hydrogel was completely healed, the output performance of TENG almost reached the level before cutting (Figure S8a,b). Figure 3g displays the measured output currents and calculated powers of the TENG under different external loading resistances at a pressure of 2.9 N and a contact frequency of 0.40 Hz, showing that the output current decreases with the increase in the external loading resistance. According to the formula $P = I^2R$, the output power of the TENG under different external loading resistances could be calculated. As the picture shows, the corresponding output power first increases and then decreases rapidly. Moreover, the optimum output power of the TENG is about 383 μW under a loading resistance of 70 MΩ. In order to facilitate the use for tiny electronic devices, the produced electric energy from the TENG by harvesting mechanical energy is usually stored in capacitors or batteries. We studied the charging performance of the capacitors with different capacities. Note that a rectifier is required to connect to the TENG to convert the alternating current generated by the TENG into direct current for charging purposes. As illustrated in Figure 3h, the smaller the capacitor capacity, the faster the increase in voltage in the charging process. The 0.22 μF capacitor voltage can be charged from 0 to 24.3 V in approximately 295 s, while the 0.33, 10, and 22 μF capacitor voltages can be charged to 11.7, 2.2, and 1.2 V,

https://doi.org/10.1021/acsomega.2c01743
ACS Omega 2022, 7, 18816−18825

respectively. The charging results show that the electrical energy generated by the TENG can be successfully stored in the capacitor, which provides the possibility for the continuous operation of the microelectronic devices.

To demonstrate the application potential of self-healing hydrogel-based TENG in wearable pressure sensors, a 2 × 2 sensor array consisting of four small-scale TENGs was constructed. It is important to analyze the response of the output performance to contact frequency and pressure. Figure 4a,b shows the output voltage and current signals of the four channels of the sensor under conditions of constant pressure (15 N) and different frequencies, respectively. It can be seen that when the contact frequency is 0.20 Hz, the output voltage of the channel 1 is 0.9 V, and the corresponding current is approximately 45 nA. As the frequency increases, the output electrical signals also increase accordingly. At 0.33 and 0.40 Hz, the output voltage/current signals are 1.3 V/56 nA and 1.8 V/68 nA, respectively. The output signals of channel 2, 3, and 4 have the same trend and similar values. Figure 4c,d further presents the output variation of the four channels at different pressures at a constant contact frequency of 0.40 Hz. Similar to the effect of contact frequency, with the increase of applied pressure from 15 to 28 N, the generated electrical signals of four channels all gradually increase from ∼1.9 V/67 nA to ∼3.4 V/94 nA. To measure the sensitivity of the pressure sensor, we have fitted the linear relationship between pressure and output voltage/current peaks at different contact frequencies. As shown in Figure 4e,f, for the pressure sensor, both the output voltage and current signals show an excellent linear relationship with applied pressures. The slope of the fitted curves represents the sensitivity of the sensor to pressure. At 0.20 Hz, the calculated sensitivities of the pressure sensor from voltage and current are 91.0 mV/N and 2.315 nA/N, respectively. When the contact frequencies are 0.33 and 0.4 Hz, the corresponding sensitivities are 97.2 mV/N/2.16 nA/N and 105.9 mV/N/1.73 nA/N, which shows good sensitivity of the pressure sensor applied under different contact frequencies.

The fabricated 2 × 2 array pressure sensor above can act as a wearable pressure sensor for motion monitoring. First, we examined the practical effect of the motion sensor, as shown in Figure 5a. A finger presses the four individual sensor units from channel 1 to 4 in sequence, then from channel 4 to 1; each channel produces the corresponding induction signals in turn. Note that no electrical signal output is detected in the unit where no force is applied. Due to the different pressures of the fingers, the generated signals also vary from 0.33 to 0.98 V. The corresponding test photos of pressing the four channels with fingers are shown in Figure 5b−e. Figure 5f is the sensor output voltage signals measured as the volunteer periodically straightens and bends his elbow; the corresponding test photos are displayed in Figure 5g,h, respectively. When the elbow is straightened, the sensor has no voltage signal output, but when the elbow is first bent and then straightened, the four channels of the sensor can simultaneously generate four similar electrical signals. Due to the different positions of each channel, the magnitude of the signal induced by it is also different, ranging from 1.69 to 2.36 V. Moreover, when the elbow is bent at different angles, each sensor unit detects different output voltage signals, showing huge application potential in monitoring motion.

4. CONCLUSIONS

In summary, this work presents a novel and simple self-healing hydrogel-based TENG and sensor for efficient mechanical harvesting and motion monitoring. Through structure design and regulation, a flexible and transparent hydrogel was prepared with excellent self-healing property. Moreover, the prepared self-healing hydrogel shows good mechanical properties without plastic deformation even at a large stretchable strain of 200%. Under a contact frequency of 0.40 Hz and a pressure of 2.9 N, the fabricated TENG generates the output electrical signals of 33.0 V and 3 μA, respectively, which can be used to charge capacitors. Comparing the output performance changes of the hydrogel-based TENG and the healed hydrogel-based TENG, it was found that the latter does not decrease significantly. As a wearable array pressure sensor based on several individual TENGs, a high sensitivity of 105.9 mV/N can be realized. Moreover, the output signals of the sensor are different under different motion states of the human body. The study demonstrates the potential application of self-healing hydrogels as triboelectric layers for TENGs and wearable triboelectric pressure sensors.

■ ASSOCIATED CONTENT

Supporting Information

The Supporting Information is available free of charge at https://pubs.acs.org/doi/10.1021/acsomega.2c01743.

FTIR spectrum of the dried self-healing hydrogel powder; high-magnification and low-magnification SEM and LSCM images of the self-healing hydrogel after freeze-drying; photographs of the self-healing hydrogels before and after cutting and stretching; high-magnification and low-magnification LSCM images of the surface of the self-healing hydrogel after the TENG was continuously working for 6 h; photographs of the self-healing hydrogels before cutting, after cutting, and after healing; comparison of measured output voltage and current signals of the self-healing hydrogel-based TENG before and after healing; and measured output voltage and current signals of the self-healing hydrogel-based TENG before cutting and during self-healing process (PDF)

■ AUTHOR INFORMATION

Corresponding Authors

Kun Zhao − *State Key Laboratory of Advanced Processing and Recycling of Nonferrous Metals, Lanzhou University of Technology, Lanzhou 730050, P. R. China*; orcid.org/0000-0002-6689-6968; Email: zhaokun@lut.edu.cn

Maocheng Liu − *School of Materials Science and Engineering, Lanzhou University of Technology, Lanzhou 730050, P. R. China*; Email: liumc@lut.edu.cn

Ding Zhang − *School of Materials Science and Engineering, National Institute for Advanced Materials, Nankai University, Tianjin 300350, P. R. China*; Email: zhangding@nankai.edu.cn

Authors

Haoran Lv − *State Key Laboratory of Advanced Processing and Recycling of Nonferrous Metals, Lanzhou University of Technology, Lanzhou 730050, P. R. China*

Jingke Meng − *State Key Laboratory of Advanced Processing and Recycling of Nonferrous Metals, Lanzhou University of Technology, Lanzhou 730050, P. R. China*

https://doi.org/10.1021/acsomega.2c01743
ACS Omega 2022, 7, 18816−18825

Zhenhua Song − *State Key Laboratory of Advanced Processing and Recycling of Nonferrous Metals, Lanzhou University of Technology, Lanzhou 730050, P. R. China*

Cheng Meng − *Jiangxi Province Key Laboratory of Polymer Micro/Nano Manufacturing and Devices, School of Chemistry, Biology and Materials Science, East China University of Technology, Nanchang 330013, P. R. China*

Complete contact information is available at: https://pubs.acs.org/10.1021/acsomega.2c01743

Author Contributions

K.Z. conceived and coordinated the study, took photos, analyzed the data, and prepared the manuscript. H.L., J.M., and Z.S. conducted the experimental work. H.L., J.M., and C.M. drew the curves and figures. All authors discussed the results and commented on this manuscript. K.Z., H.L., M.L., and D.Z. wrote the manuscript with contributions from all co-authors. All authors have approved the final version of the manuscript.

Notes

The authors declare no competing financial interest.

■ ACKNOWLEDGMENTS

This work was supported by the National Natural Science Foundation of China (grant no.52065038), the Outstanding Youth Foundation of Gansu Province (grant no. 21JR7RA275), the Tamarisk Outstanding Young Talents Program of Lanzhou University of Technology in 2020 (grant no. 062004), a project funded by the China Postdoctoral Science Foundation (grant no. 2021M693836), the Outstanding Young Talents Training Program of State Key Laboratory of Advanced Processing and Recycling of Nonferrous Metals (grant no. 2018004), and the Natural Science Foundation of Jiangxi Province (grant no. 20202BABL214058).

■ REFERENCES

(1) Lipomi, D. J.; Vosgueritchian, M.; Tee, B. C.-K.; Hellstrom, S. L.; Lee, J. A.; Fox, C. H.; Bao, Z. Skin-Like Pressure and Strain Sensors Based on Transparent Elastic Films of Carbon Nanotubes. *Nat. Nanotechnol.* **2011**, *6*, 788−792.

(2) Rogers, J. A.; Someya, T.; Huang, Y. Materials and Mechanics for Stretchable Electronics. *Science* **2010**, *327*, 1603−1607.

(3) Morin, S. A.; Shepherd, R. F.; Kwok, S. W.; Stokes, A. A.; Nemiroski, A.; Whitesides, G. M. Camouflage and Display for Soft Machines. *Science* **2012**, *337*, 828−832.

(4) Shepherd, R. F.; Ilievski, F.; Choi, W.; Morin, S. A.; Stokes, A. A.; Mazzeo, A. D.; Chen, X.; Wang, M.; Whitesides, G. M. Multigait Soft Robot. *Proc. Natl. Acad. Sci. U.S.A.* **2011**, *108*, 20400−20403.

(5) Kim, D.-H.; Lu, N.; Ma, R.; Kim, Y.-S.; Kim, R.-H.; Wang, S.; Wu, J.; Won, S. M.; Tao, H.; Islam, A.; Yu, K. J.; Kim, T.-I.; Chowdhury, R.; Ying, M.; Xu, L.; Li, M.; Chung, H.-J.; Keum, H.; McCormick, M.; Liu, P.; Zhang, Y.-W.; Omenetto, F. G.; Huang, Y.; Coleman, T.; Rogers, J. A. Epidermal Electronics. *Science* **2011**, *333*, 838−843.

(6) Gao, W.; Emaminejad, S.; Nyein, H. Y. Y.; Challa, S.; Chen, K.; Peck, A.; Fahad, H. M.; Ota, H.; Shiraki, H.; Kiriya, D.; Lien, D.-H.; Brooks, G. A.; Davis, R. W.; Javey, A. Fully Integrated Wearable Sensor Arrays for Multiplexed in Situ Perspiration Analysis. *Nature* **2016**, *529*, 509−514.

(7) Chen, G.; Li, Y.; Bick, M.; Chen, J. Smart Textiles for Electricity Generation. *Chem. Rev.* **2020**, *120*, 3668−3720.

(8) Zhang, D.; Wang, D.; Xu, Z.; Zhang, X.; Yang, Y.; Guo, J.; Zhang, B.; Zhao, W. Diversiform Sensors and Sensing Systems Driven by Triboelectric and Piezoelectric Nanogenerators. *Coord. Chem. Rev.* **2021**, *427*, 213597.

(9) Li, Z.; Chen, J.; Guo, H.; Fan, X.; Wen, Z.; Yeh, M.-H.; Yu, C.; Cao, X.; Wang, Z. L. Triboelectrification-Enabled Self-Powered Detection and Removal of Heavy Metal Ions in Wastewater. *Adv. Mater.* **2016**, *28*, 2983−2991.

(10) Yu, X.; Shou, W.; Mahajan, B. K.; Huang, X.; Pan, H. Materials, Processes, and Facile Manufacturing for Bioresorbable Electronics: A Review. *Adv. Mater.* **2018**, *30*, 1707624.

(11) Wang, Z.; Zhang, B.; Guan, D. Take Responsibility for Electronic-Waste Disposal. *Nature* **2016**, *536*, 23−25.

(12) Cao, X.; Jie, Y.; Wang, N.; Wang, Z. L. Triboelectric Nanogenerators Driven Self-Powered Electrochemical Processes for Energy and Environmental Science. *Adv. Energy Mater.* **2016**, *6*, 1600665.

(13) Stone, R. Confronting a Toxic Blowback from the Electronics Trade. *Science* **2009**, *325*, 1055.

(14) Ogunseitan, O. A.; Schoenung, J. M.; Saphores, J.-D. M.; Shapiro, A. A. The Electronics Revolution: From E-Wonderland to E-Wasteland. *Science* **2009**, *326*, 670−671.

(15) Fan, F.-R.; Tian, Z.-Q.; Wang, Z. L. Flexible Triboelectric Generator. *Nano Energy* **2012**, *1*, 328−334.

(16) Zhang, L.; Su, C.; Cui, X.; Li, P.; Wang, Z.; Gu, L.; Tang, Z. Free-Standing Triboelectric Layer-Based Full Fabric Wearable Nanogenerator for Efficient Mechanical Energy Harvesting. *ACS Appl. Electron. Mater.* **2020**, *2*, 3366−3372.

(17) Guan, D.; Xu, G.; Xia, X.; Wang, J.; Zi, Y. Boosting the Output Performance of the Triboelectric Nanogenerator through the Nonlinear Oscillator. *ACS Appl. Mater. Interfaces* **2021**, *13*, 6331−6338.

(18) Zhang, H.; Yang, C.; Yu, Y.; Zhou, Y.; Quan, L.; Dong, S.; Luo, J. Origami-Tessellation-Based Triboelectric Nanogenerator for Energy Harvesting with Application in Road Pavement. *Nano Energy* **2020**, *78*, 105177.

(19) Chen, P.; An, J.; Shu, S.; Cheng, R.; Nie, J.; Jiang, T.; Wang, Z. L. Super-Durable, Low-Wear, and High-Performance Fur-Brush Triboelectric Nanogenerator for Wind and Water Energy Harvesting for Smart Agriculture. *Adv. Energy Mater.* **2021**, *11*, 2003066.

(20) Wang, F.; Wang, Z.; Zhou, Y.; Fu, C.; Chen, F.; Zhang, Y.; Lu, H.; Wu, Y.; Chen, L.; Zheng, H. Windmill-Inspired Hybridized Triboelectric Nanogenerators Integrated with Power Management Circuit for Harvesting Wind and Acoustic Energy. *Nano Energy* **2020**, *78*, 105244.

(21) Salauddin, M.; Rana, S. M. S.; Sharifuzzaman, M.; Rahman, M. T.; Park, C.; Cho, H.; Maharjan, P.; Bhatta, T.; Park, J. Y. A Novel MXene/Ecoflex Nanocomposite-Coated Fabric as a Highly Negative and Stable Friction Layer for High-Output Triboelectric Nanogenerators. *Adv. Energy Mater.* **2021**, *11*, 2002832.

(22) Chen, H.; Wang, J.; Ning, A. Optimization of a Rolling Triboelectric Nanogenerator Based on the Nano-Micro Structure for Ocean Environmental Monitoring. *ACS Omega* **2021**, *6*, 21059−21065.

(23) Yang, H.; Deng, M.; Tang, Q.; He, W.; Hu, C.; Xi, Y.; Liu, R.; Wang, Z. L. A Nonencapsulative Pendulum-Like Paper-Based Hybrid Nanogenerator for Energy Harvesting. *Adv. Energy Mater.* **2019**, *9*, 1901149.

(24) Chen, C.; Wen, Z.; Shi, J.; Jian, X.; Li, P.; Yeow, J. T. W.; Sun, X. Micro Triboelectric Ultrasonic Device for Acoustic Energy Transfer and Signal Communication. *Nat. Commun.* **2020**, *11*, 4143.

(25) Zhao, H.; Xiao, X.; Xu, P.; Zhao, T.; Song, L.; Pan, X.; Mi, J.; Xu, M.; Wang, Z. L. Dual-Tube Helmholtz Resonator-Based Triboelectric Nanogenerator for Highly Efficient Harvesting of Acoustic Energy. *Adv. Energy Mater.* **2019**, *9*, 1902824.

(26) Wang, S.; Liu, S.; Zhou, J.; Li, F.; Li, J.; Cao, X.; Li, Z.; Zhang, J.; Li, B.; Wang, Y.; Gong, X. Advanced Triboelectric Nanogenerator with Multi-Mode Energy Harvesting and Anti-Impact Properties for Smart Glove and Wearable E-Textile. *Nano Energy* **2020**, *78*, 105291.

(27) Liu, J.; Tang, W.; Meng, X.; Zhan, L.; Xu, W.; Nie, Z.; Wang, Z. Improving the Performance of the Mini 2000 Mass Spectrometer with a Triboelectric Nanogenerator Electrospray Ionization Source. *ACS Omega* **2018**, *3*, 12229−12234.

(28) Tantraviwat, D.; Ngamyingyoud, M.; Sripumkhai, W.; Pattamang, P.; Rujijanagul, G.; Inceesungvorn, B. Tuning the Dielectric Constant and Surface Engineering of a $BaTiO_3$/Porous PDMS

Composite Film for Enhanced Triboelectric Nanogenerator Output Performance. *ACS Omega* **2021**, *6*, 29765−29773.
(29) Kamilya, T.; Sarkar, P. K.; Acharya, S. Unveiling Peritoneum Membrane for a Robust Triboelectric Nanogenerator. *ACS Omega* **2019**, *4*, 17684−17690.
(30) Jie, Y.; Jia, X.; Zou, J.; Chen, Y.; Wang, N.; Wang, Z. L.; Cao, X. Natural Leaf Made Triboelectric Nanogenerator for Harvesting Environmental Mechanical Energy. *Adv. Energy Mater.* **2018**, *8*, 1703133.
(31) Jiao, J.; Lu, Q.; Wang, Z.; Qin, Y.; Cao, X. Sandwich as a Triboelectric Nanogenerator. *Nano Energy* **2021**, *79*, 105411.
(32) Chen, H.; Zhang, S.; Zou, Y.; Zhang, C.; Zheng, B.; Huang, C.; Zhang, B.; Xing, C.; Xu, Y.; Wang, J. Performance-Enhanced Flexible Triboelectric Nanogenerator Based on Gold Chloride-Doped Graphene. *ACS Appl. Electron. Mater.* **2020**, *2*, 1106−1112.
(33) Wang, J.; Li, X.; Zi, Y.; Wang, S.; Li, Z.; Zheng, L.; Yi, F.; Li, S.; Wang, Z. L. A Flexible Fiber-Based Supercapacitor−Triboelectric-Nanogenerator Power System for Wearable Electronics. *Adv. Mater.* **2015**, *27*, 4830−4836.
(34) Ning, C.; Dong, K.; Cheng, R.; Yi, J.; Ye, C.; Peng, X.; Sheng, F.; Jiang, Y.; Wang, Z. L. Flexible and Stretchable Fiber-Shaped Triboelectric Nanogenerators for Biomechanical Monitoring and Human-Interactive Sensing. *Adv. Funct. Mater.* **2021**, *31*, 2006679.
(35) Shi, L.; Zhao, Y.; Xie, Q.; Fan, C.; Hilborn, J.; Dai, J.; Ossipov, D. A. Moldable Hyaluronan Hydrogel Enabled by Dynamic Metal−Bisphosphonate Coordination Chemistry for Wound Healing. *Adv. Healthcare Mater.* **2018**, *7*, 1700973.
(36) Mredha, M. T. I.; Guo, Y. Z.; Nonoyama, T.; Nakajima, T.; Kurokawa, T.; Gong, J. P. A Facile Method to Fabricate Anisotropic Hydrogels with Perfectly Aligned Hierarchical Fibrous Structures. *Adv. Mater.* **2018**, *30*, 1704937.
(37) Zhao, X.; Chen, F.; Li, Y.; Lu, H.; Zhang, N.; Ma, M. Bioinspired Ultra-Stretchable and Anti-Freezing Conductive Hydrogel Fibers with Ordered and Reversible Polymer Chain Alignment. *Nat. Commun.* **2018**, *9*, 3579.
(38) Yao, B.; Wang, H.; Zhou, Q.; Wu, M.; Zhang, M.; Li, C.; Shi, G. Ultrahigh-Conductivity Polymer Hydrogels with Arbitrary Structures. *Adv. Mater.* **2017**, *29*, 1700974.
(39) Huang, L.-B.; Dai, X.; Sun, Z.; Wong, M.-C.; Pang, S.-Y.; Han, J.; Zheng, Q.; Zhao, C.-H.; Kong, J.; Hao, J. Environment-Resisted Flexible High Performance Triboelectric Nanogenerators Based on Ultrafast Self-Healing Non-Drying Conductive Organohydrogel. *Nano Energy* **2021**, *82*, 105724.
(40) Qi, J.; Wang, A. C.; Yang, W.; Zhang, M.; Hou, C.; Zhang, Q.; Li, Y.; Wang, H. Hydrogel-Based Hierarchically Wrinkled Stretchable Nanofibrous Membrane for High Performance Wearable Triboelectric Nanogenerator. *Nano Energy* **2020**, *67*, 104206.
(41) Pu, X.; Liu, M.; Chen, X.; Sun, J.; Du, C.; Zhang, Y.; Zhai, J.; Hu, W.; Wang, Z. L. Ultrastretchable, Transparent Triboelectric Nanogenerator as Electronic Skin for Biomechanical Energy Harvesting and Tactile Sensing. *Sci. Adv.* **2017**, *3*, 1700015.
(42) Sun, H.; Zhao, Y.; Wang, C.; Zhou, K.; Yan, C.; Zheng, G.; Huang, J.; Dai, K.; Liu, C.; Shen, C. Ultra-Stretchable, Durable and Conductive Hydrogel with Hybrid Double Network as High Performance Strain Sensor and Stretchable Triboelectric Nanogenerator. *Nano Energy* **2020**, *76*, 105035.
(43) Sun, W.; Luo, N.; Liu, Y.; Li, H.; Wang, D. A New Self-Healing Triboelectric Nanogenerator Based on Polyurethane Coating and Its Application for Self-Powered Cathodic Protection. *ACS Appl. Mater. Interfaces* **2022**, *14*, 10498−10507.
(44) Luo, N.; Feng, Y.; Wang, D.; Zheng, Y.; Ye, Q.; Zhou, F.; Liu, W. New Self-Healing Triboelectric Nanogenerator Based on Simultaneous Repair Friction Layer and Conductive Layer. *ACS Appl. Mater. Interfaces* **2020**, *12*, 30390−30398.
(45) Guo, Z.; Ma, W.; Gu, H.; Feng, Y.; He, Z.; Chen, Q.; Mao, X.; Zhang, J.; Zheng, L. PH-Switchable and Self-Healable Hydrogels Based on Ketone Type Acylhydrazone Dynamic Covalent Bonds. *Soft Matter* **2017**, *13*, 7371−7380.
(46) Song, G.; Zhang, L.; He, C.; Fang, D.-C.; Whitten, P. G.; Wang, H. Facile Fabrication of Tough Hydrogels Physically Cross-Linked by Strong Cooperative Hydrogen Bonding. *Macromolecules* **2013**, *46*, 7423−7435.

https://doi.org/10.1021/acsomega.2c01743
ACS Omega 2022, 7, 18816−18825